© The American Society of Gene & Cell Therapy

Aptamer Against Mannose-capped Lipoarabinomannan Inhibits Virulent *Mycobacterium tuberculosis* Infection in Mice and Rhesus Monkeys

Qin Pan[1], Qilong Wang[1], Xiaoming Sun[1], Xianru Xia[1], Shimin Wu[2], Fengling Luo[1] and Xiao-Lian Zhang[1]

[1]*State Key Laboratory of Virology, Department of Immunology, Hubei Province Key Laboratory of Allergy and Immunology, Wuhan University School of Medicine, Wuhan, China;* [2]*Department of Laboratory Medicine, Wuhan Medical Treatment Center, Wuhan, China*

The major surface lipoglycan of *Mycobacterium tuberculosis* (*M. tb*), mannose-capped lipoarabinomannan (ManLAM), is an immunosuppressive epitope of *M. tb*. We used systematic evolution of ligands by exponential enrichment (SELEX) to generate an aptamer (ZXL1) that specifically bound to ManLAM from the virulent *M. tb* strain H37Rv. Aptamer ZXL1 had the highest binding affinity, with an equilibrium dissociation constant (K_d) of 436.3±37.84 nmol/l, and competed with the mannose receptor for binding to ManLAM and *M. tb* H37Rv. ZXL1 significantly inhibited the ManLAM-induced immunosuppression of $CD11c^+$ dendritic cells (DCs) and enhanced the *M. tb* antigen–presenting activity of DCs for naive $CD4^+$ Th1 cell activation. More importantly, we demonstrated that injection of aptamer ZXL1 significantly reduced the progression of *M. tb* H37Rv infections and bacterial loads in lungs of mice and rhesus monkeys. These results suggest that the aptamer ZXL1 is a new potential antimycobacterial agent and tuberculosis vaccine immune adjuvant.

Received 25 May 2013; accepted 20 February 2014; advance online publication 25 March 2014. doi:10.1038/mt.2014.31

INTRODUCTION

Tuberculosis (TB) is a formidable public health challenge that contributes significantly to illness and death around the world. The World Health Organization (WHO) estimated that there were 8.5–9.2 million TB cases and 1.2–1.5 million TB-associated deaths globally in 2011.[1] An attenuated strain vaccine of *Mycobacterium bovis*, termed Bacillus Calmette–Guérin (BCG), the only available TB vaccine, decreases TB in children but gives little protection against TB in adults.[2] Other major threats to controlling TB are extensively drug-resistant TB (XDR-TB) and increased prevalence of multidrug-resistant TB, which have emerged in patients infected with the human immunodeficiency virus.[3] Therefore, potent new anti-TB drugs without cross-resistance to known antimycobacterial agents are urgently needed.

Both macrophages and dendritic cells (DCs) are primary targets for *Mycobacterium tuberculosis* (*M. tb*) infection.[4,5] DCs are potent antigen-presenting cells that activate naive T cells and determine the nature of the antimycobacterial response. Mannose-capped lipoarabinomannan (ManLAM) is a lipoglycan serving as a major cell wall component. Its function has been described to inactivate macrophages, scavenge oxidative radicals, and mediate immunosuppressive effects. *M. tb* ManLAM inhibits phagosome maturation in macrophages, DC maturation, and $CD4^+$ T-cell activation.[6–8] ManLAM induces immunosuppression by inhibition of DC maturation, increase of interleukin (IL)-10 production by DCs, and depression of its IL-12 cytokine production.[8] Immune mediators, such as IL-12 and interferon (IFN)-γ, activate macrophages and T cells and promote bacterial killing. An orchestrated Th1-type cellular immune response involving $CD4^+$ and $CD8^+$ T cells is required to effectively inhibit *M. tb* infection.

Aptamers are single-stranded oligonucleotides with lengths of tens of nucleotides, and these are generated by an *in vitro* selection process called systematic evolution of ligands by exponential enrichment (SELEX), which was first reported in 1990.[9,10] Aptamers have high affinity and specificity toward recognized targets. Aptamers have been used in numerous investigations as therapeutic or diagnostic tools.[11,12] However, aptamers against ManLAM have not been reported.

In this study, we used SELEX technology to screen and identify single-stranded DNA (ssDNA) aptamers that specifically bound to ManLAM isolated from the virulent *M. tb* strain H37Rv. The selected aptamer ZXL1 had the highest binding affinity for ManLAM and *M. tb* H37Rv, and it protected mice and rhesus monkeys from *M. tb* infection.

RESULTS

High-affinity aptamers against ManLAM were generated by SELEX

ManLAM from *M. tb* H37Rv was purified and identified by high-performance liquid chromatography, sodium dodecyl sulfate–polyacrylamide gel electrophoresis(silver staining), and western blotting (**Figure 1a**). A random single-stranded (ss) DNA library (~10^{14} aptamers) was screened for efficacy of binding to ManLAM. The ssDNAs bound to ManLAM coated on the well were selected as described in the Methods section. Candidate aptamers were enriched at each selection round by amplification using polymerase

The first two authors contributed equally to this work.

Correspondence: *Xiao-Lian Zhang, Department of Immunology, Wuhan University School of Medicine, Wuhan 430071, P. R. China.*
E-mail: zhangxiaolian@whu.edu.cn

© The American Society of Gene & Cell Therapy

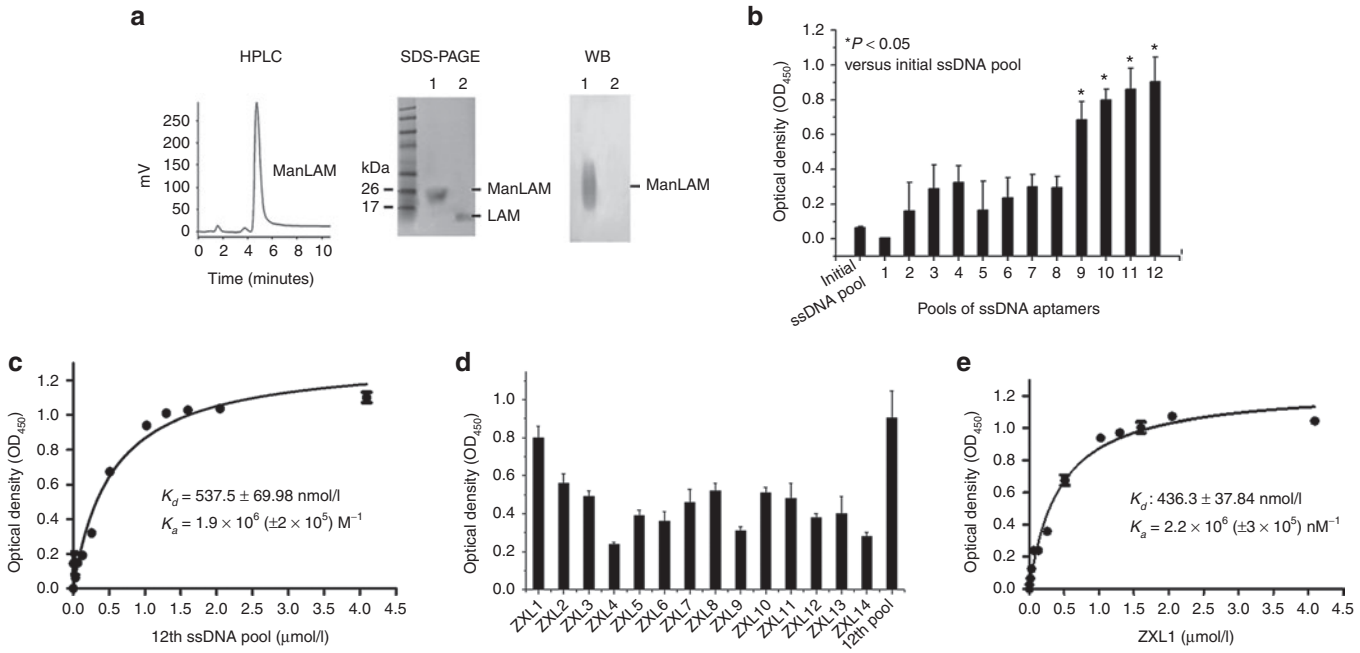

Figure 1 High-affinity aptamers for mannose-capped lipoarabinomannan (ManLAM) were generated by systematic evolution of ligands by exponential enrichment (SELEX). (**a**) Identification of the purified ManLAM from *Mycobacterium tuberculosis* (*M. tb*) H37Rv by high-performance liquid chromatography (HPLC) showing the final preparation of ManLAM, sodium dodecyl sulfate–polyacrylamide gel electrophoresis (silver staining), and western blot (WB) analyses. (**b**) After 12 rounds of screening against ManLAM, single-stranded DNA (ssDNA) pools from each round were analyzed for their binding to ManLAM by enzyme-linked oligonucleotide assay. Aptamer pools (2 μmol/l) were incubated in wells coated with ManLAM (40 μg/ml in phosphate-buffered saline). In the background control, 40 μg/ml of ManLAM was coated on the wells, but none of the ssDNA aptamers were added. For each sample, the optical density at 450 nm (OD_{450}) of the background control was subtracted from the OD_{450} of experimental sample.*$P < 0.05$ versus initial ssDNA pool. All data are shown as the means ± SEMs ($n = 3$). (**c**) Binding of the 12th ssDNA pool to ManLAM. The 12th-round pool of ssDNA was incubated in wells coated with ManLAM. All data are shown as the means ± SEMs ($n = 3$). The K_d of 537.5 ± 69.98 nmol/l was determined as described in the Methods section. (**d**) Binding of the single aptamers ZXL1–ZXL14 to ManLAM. The single aptamers ZXL1–ZXL14 (2 μmol/l) were, respectively, incubated in wells coated with ManLAM. All data are shown as the means ± SEMs ($n = 3$). (**e**) Analysis of binding of ZXL1 to ManLAM. ZXL1 was added and incubated in the wells coated with ManLAM. All data are shown as the means ± SEMs ($n = 3$). The K_d of 436.3 ± 37.84 nmol/l was established as described in the Methods section.

chain reaction. Enrichment of the selection pool through successive rounds of selection was monitored by enzyme-linked oligonucleotide assay (ELONA) (**Figure 1b**). Compared with other pools, the 12th-round ssDNA pool demonstrated the strongest binding to ManLAM (**Figure 1b**), which was dose dependent for the aptamers (**Figure 1c**). The dissociation constant (K_d values) of the 12th-round pool was determined to be 537.5 ± 69.98 nmol/l (**Figure 1c**). As the SELEX progressed, the latter aptamer pool showed increased specificity but decreased sequence diversity compared with the former pool.[13,14] According to our data, the binding ability of round-9 aptamer pool was sharply increased by nearly 200% compared with that of round-8 aptamer pool (**Figure 1b**). However, from round 10 to round 12, the binding ability of the former pool was increased by less than 10% compared with that of the latter pool (**Figure 1b**). These data suggested that the affinity of the 12th-round pool might be close to saturation. Therefore, we decided to stop the selection at the 12th round.

The 12th-round ssDNA pool was then cloned into pUC19, and individual clones were randomly selected and sequenced (**Supplementary Table S1**). The consensus sequences (in red color and presented 13 times in the 18 clones) were CxxxC in one family and GxxxxxTG in the other family. The clone ZXL1 had the highest frequency and appeared four times among all aptamers. ZXL1 showed the highest ability to bind to ManLAM, whereas ZXL4 showed the weakest binding to ManLAM (**Figure 1d**). As determined by ELONA, the K_d value of ZXL1 was 436.3 ± 37.84 nmol/l (**Figure 1e**). Secondary structure analysis demonstrated that the consensus sequence (CxxxC) of ZXL1 was located at the terminal loop of the stem–loop structure (**Supplementary Figure S1**).

The selected aptamer ZXL1 specifically bound to *M. tb* H37Rv

The binding specificity of ZXL1 was validated using various bacteria, including *M. tb* H37Rv, BCG, *Mycobacterium smegmatis*, *M. intracellulare*, *M. avium*, *Pseudomonas aeruginosa*, *Staphylococcus aureus*, *Escherichia coli*, *Staphylococcus albus*, *Micrococcus luteus*, and *Salmonella typhimurium* C5. By using ELONA analysis, binding of ZXL1 to *M. tb* H37Rv was significantly higher than its binding to other bacteria (**Figure 2a**). The aptamer control (ZXL4) did not bind to *M. tb* H37Rv (**Figure 2a**). Flow cytometry (FCM) demonstrated that ZXL1 bound to virulent *M. tb* H37Rv much more strongly (52.2%) than to the other *Mycobacteria* strains tested, *M. smegmatis* (2.5%) and BCG (13.9%) (**Figure 2b**). Confocal microscopy showed that both rhodamine B dye and 6-carboxyfluorescein (FAM)-labeled ZXL1 bound to the virulent *M. tb* strain H37Rv, but FAM-labeled ZXL1 did not bind to nonvirulent BCG (**Figure 2c**). Flow cytometry (**Figure 2b**) and confocal microscopy (**Figure 2c**) analyses

© The American Society of Gene & Cell Therapy

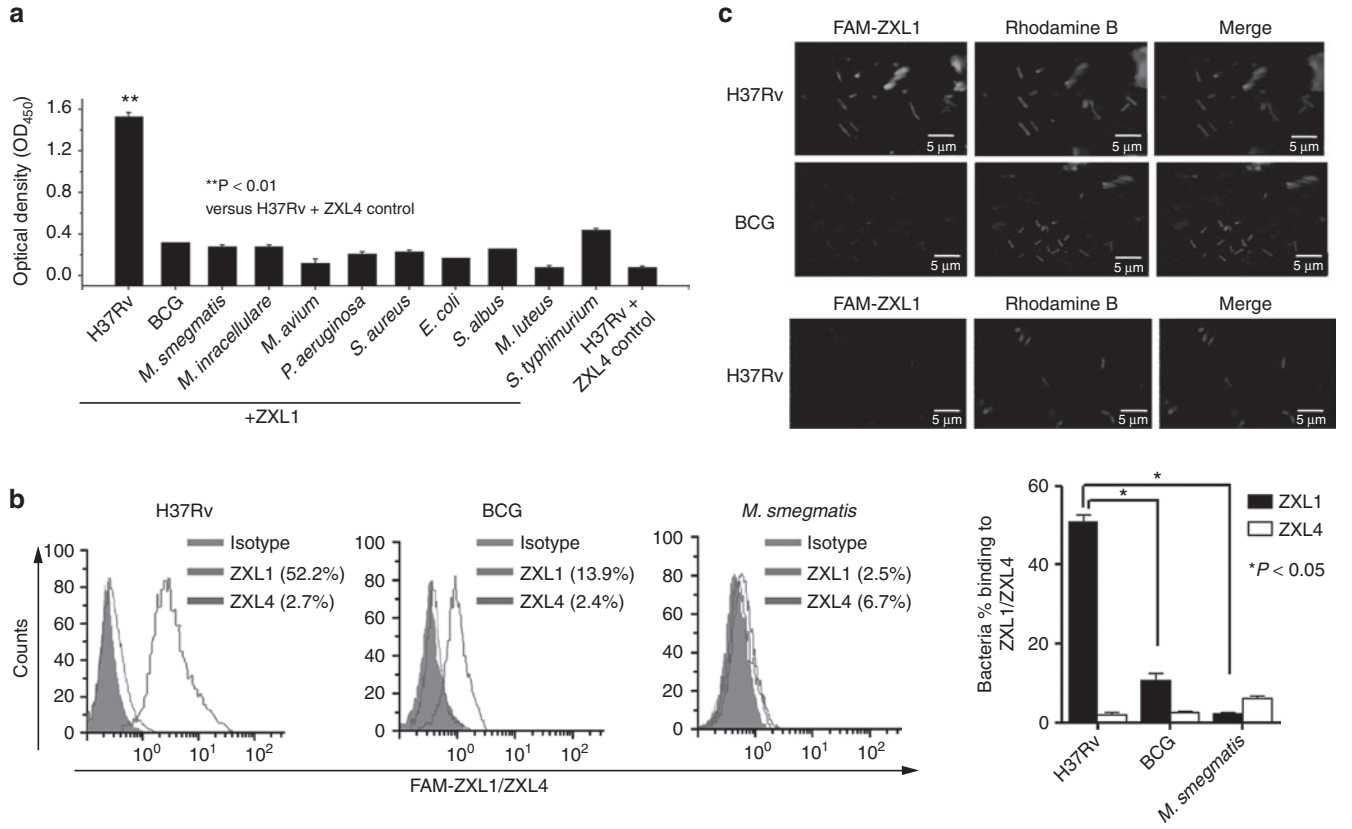

Figure 2 The selected aptamer ZXL1 bound specifically to *Mycobacterium tuberculosis* (*M. tb*) H37Rv. (**a**) Binding of ZXL1 to bacteria was evaluated by enzyme-linked oligonucleotide assay. Biotin-labeled ZXL1 was incubated (2 μmol/l) in wells coated with 1×10^5 colony forming units (CFUs) of the bacteria. $^{**}P < 0.01$ versus *M. tb.* H37Rv+ZXL4 control. All data are shown as the means ± SEMs ($n = 3$). (**b**) Binding of ZXL1 to *M. tb* H37Rv, Bacillus Calmette–Guérin (BCG), and *M. smegmatis* was evaluated by flow cytometry (FCM) analysis. Then, 1×10^7 CFUs of the bacteria were fixed with 70% ethanol and incubated with 6-carboxyfluorescein (FAM)-labeled ZXL1 (5 μmol/l) for FCM analysis. $^{*}P < 0.05$ versus BCG and *M. smegmatis*. All data are shown as the means ± SEMs ($n = 3$). (**c**) Binding of ZXL1 to *M. tb* H37Rv and BCG was evaluated by confocal microscopy. Thus, 1×10^5 CFUs of the bacteria were coated onto slides and incubated with FAM-labeled ZXL1 (5 μmol/l) for confocal microscopy analysis.

showed that the aptamer control (ZXL4) did not bind to both H37Rv and BCG. Altogether, these data strongly demonstrated that ZXL1 specifically bound to *M. tb* H37Rv.

ZXL1 competed with the mannose receptor for binding to ManLAM and *M. tb* H37Rv

The mannose receptor (MR) and the DC-specific intracellular adhesion molecule 3 (ICAM-3)-grabbing nonintegrin (DC-SIGN) are possible receptors for ManLAM.[8,15] We investigated whether ZXL1 could block *M. tb*–host cell interactions and determined the host cell receptor–ManLAM connections disrupted by ZXL1. We used human MRp1 (from the membrane-distal cysteine-rich domain (Cys-MR) of human MR), mouse MRp1 (from the Cys-MR of mouse MR), MRp2 (conserved amino acids from a carbohydrate-recognition domain CRD4 for both human and mouse MR), DC-SIGNp1, and DC-SIGNp2 (both from the C-type lectin domain of human DC-SIGN) as competitors in competitive ELONAs (**Supplementary Table S2**).[16,17]

In competitive ELONAs, *M. tb* H37Rv/ManLAM was coated on the plate and incubated with ZXL1 in the presence of competitors, and washes were performed to remove unbound aptamers/competitors. Binding of ZXL1 to *M. tb* H37Rv/ ManLAM was detected. As shown in **Figure 3a**, human MRp1 and MRp2 inhibited binding of ZXL1 to *M. tb* H37Rv, but mouse MRp1, DC-SIGNp1, and DC-SIGNp2 did not disrupt binding of ZXL1. We then used human MRp1 or MRp2 to compete with ZXL1 for binding to ManLAM or *M. tb* H37Rv, and the results showed that both human MRp1 and MRp2 interfered with binding of ZXL1 (**Figure 3b**). When these two competitors increased, the binding of ZXL1 to ManLAM (or *M. tb* H37Rv) was reduced. The interference by human MRp1 was similar to that by MRp2 because both 50 μmol/l human MRp1 and 50 μmol/l MRp2 reduced the binding of 2 μmol/l ZXL1 by nearly 50% (**Figure 3b**). These data suggested that ZXL1 inhibited MR binding to *M. tb* H37Rv. Our data also demonstrated that ManLAM blocked binding of aptamer ZXL1 to ManLAM coated on the well in a dose-dependent manner (**Figure 3c**). As shown in **Figure 3c**, in the presence of about 2.5 μmol/l soluble ManLAM, binding of ZXL1 to ManLAM coated on the well was reduced to 50% (half-maximal inhibitory concentration, IC_{50} = 2.5 μmol/l). We used GraphPad Prism (GraphPad Software, San Diego, CA) to perform nonlinear curve-fitting analysis. The K_i (the inhibition constant) was estimated to be 450.3 nmol/l, and the 95% confidence interval of K_i value was 189–1,074 nmol/l. Regarding the relationship between K_i and K_d ($K_i = IC_{50} / (1 + ([L] / K_d)$,[18] where [L] is the concentration of the biotin-labeled ZXL1 used), the evaluated K_d value was 438 nmol/l, and the 95% confidence

© The American Society of Gene & Cell Therapy

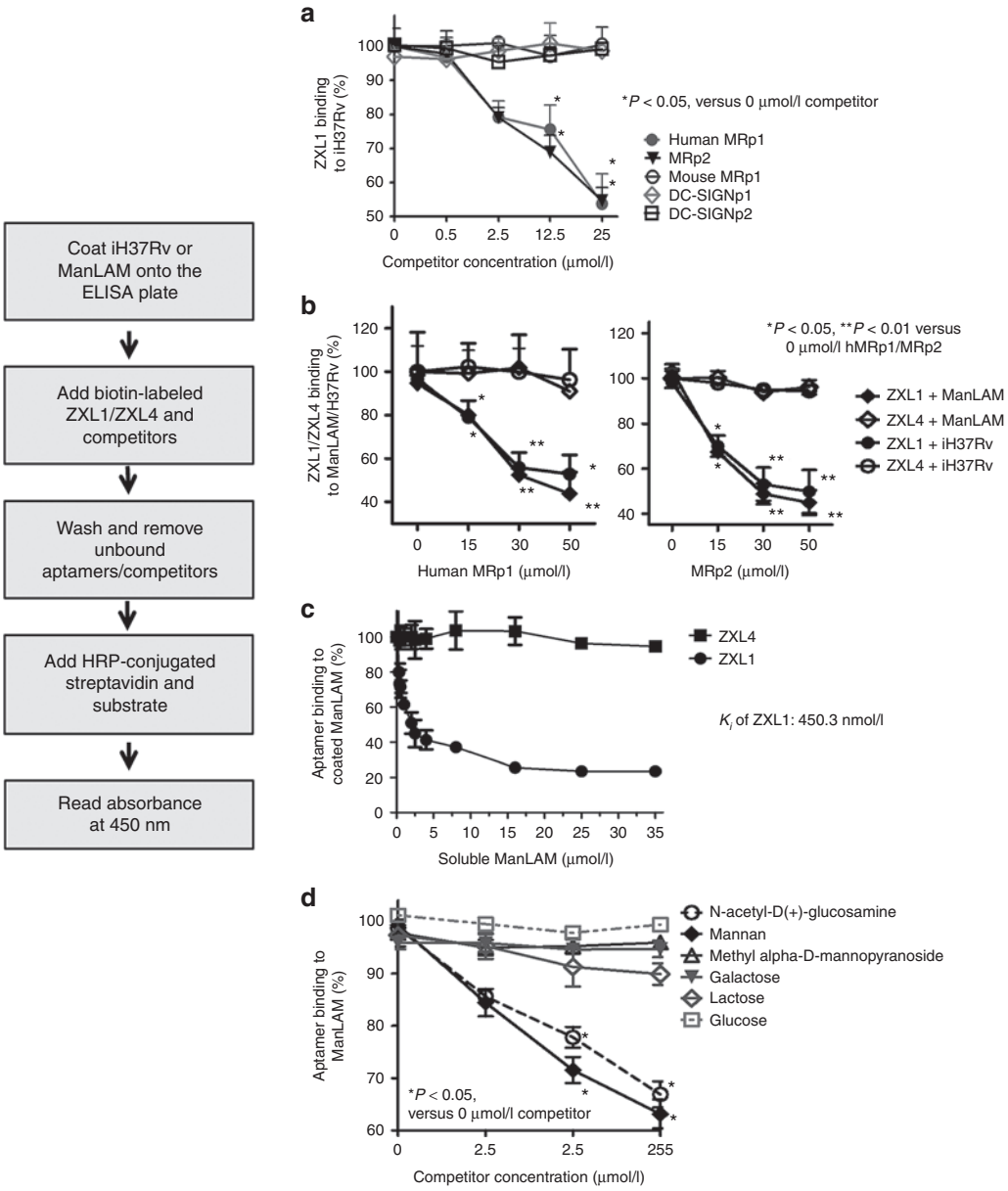

Figure 3 ZXL1 competed with mannose receptor (MR) for binding to mannose-capped lipoarabinomannan (ManLAM) or *Mycobacterium tuberculosis (M. tb)* H37Rv. ManLAM (10 μg/ml in phosphate-buffered saline) or heat-inactivated *M. tb* H37Rv (1×10^6 colony forming units (CFUs)/ml) was coated on an enzyme-linked immunosorbent assay plate, and 2 μmol/l of biotin-labeled ZXL1 and competitors were added and incubated. In the background control, the ManLAM (or heat-inactivated *M. tb* H37Rv) was coated on the wells, but none of the single-stranded DNA aptamers were added. For each sample, the optical density at 450 nm (OD_{450}) of the background control was subtracted from the OD_{450} of the experimental sample. (**a**) Human MRp1 and MRp2 inhibited binding of ZXL1 to *M. tb* H37Rv. Percentage binding: OD_{450} value of 0.5, 2.5, 12.5, or 25 μmol/l competitor group/OD_{450} value of 0 μmol/l competitor group. *$P < 0.05$ versus 0 μmol/l competitor group. All data are shown as the means ± SEMs ($n = 3$). (**b**) Human MRp1 and MRp2 inhibited binding of ZXL1 to ManLAM/*M. tb* H37Rv. Percentage binding: OD_{450} value of 15, 30, or 50 μmol/l human MRp1 (or MRp2) group/OD_{450} value of 0 μmol/l human MRp1 (or MRp2) group; *$P < 0.05$, **$P < 0.01$ versus 0 μmol/l human MRp1 (or MRp2) group. All data are shown as the means ± SEMs ($n = 3$). (**c**) Soluble ManLAM inhibited binding of ZXL1 to ManLAM coated on the well. Percentage binding: OD_{450} value of ManLAM competitor group/OD_{450} value of 0 μmol/l ManLAM competitor group. All data are shown as the means ± SEMs ($n = 3$). (**d**) Mannan and *N*-acetyl-D(+)-glucosamine inhibited binding of ZXL1 to ManLAM. Percentage binding: OD_{450} value of 2.5, 25, or 250 μmol/l carbohydrate competitor group/OD_{450} value of 0 μmol/l carbohydrate competitor group. *$P < 0.05$ versus 0 μmol/l carbohydrate competitor group. All data are shown as the means ± SEMs ($n = 3$).

interval of K_d was between 160 and 1,500 nmol/l, which was consistent with the calculated K_d of 436.3 ± 37.84 nmol/l, as shown in **Figure 1e**.

The MR interacts with a diverse array of carbohydrate ligands.[19] Therefore, several sugar competitors were used to determine the glycan motifs in ManLAM that were bound by ZXL1. Mannan and *N*-acetyl-D(+)-glucosamine partially inhibited binding of ZXL1 to ManLAM in a dose-dependent manner, whereas glucose, galactose, and lactose did not inhibit the binding (**Figure 3d**). We speculated that ZXL1 bound to the mannan and *N*-acetyl-D(+)-glucosamine–rich domain of ManLAM, consequently disrupting the interaction of MR with ManLAM. We have not found any

© The American Society of Gene & Cell Therapy

interference effect of competitors on the binding of the negative control ZXL4 to ManLAM or *M. tb* H37Rv (**Supplementary Figures S2 and S3**).

ZXL1 enhanced the DC maturation

The MR is a C-type lectin carbohydrate-binding protein primarily present on the surface of macrophages and DCs. MRs enable DCs to take up mannosylated proteins for processing and antigen presentation.[20] It has been reported that ManLAM prevents lipopolysaccharide (LPS)-induced DC maturation.[8] To investigate whether ZXL1 inhibited ManLAM-induced DC suppression, DCs derived from BALB/c mice or healthy blood donors were exposed to LPS in the presence of ManLAM or ManLAM plus ZXL1. DC maturation markers were analyzed by FCM.

As shown in **Figure 4**, ManLAM downregulated $CD11c^+$ DC maturation stimulated by LPS. The addition of ZXL1 increased expression of both mouse and human DC maturation markers, including Cluster of Differentiation (CD) 80, CD83, CD86, CD40, and major histocompatibility complex (MHC-II); particularly, the mean fluorescence intensities of MHC-II were increased by 50% (mouse DC) and 40% (human DC) (**Figure 4**). The negative control ZXL4 had almost no effect on DC maturation (**Figure 4**). Thus, these data suggested that binding of ZXL1 to ManLAM interfered with the connection between ManLAM and DCs and reversed ManLAM-induced immunosuppression of DCs.

ZXL1 enhanced antigen presentation by DCs and functional naive $CD4^+$ T-cell responses

Mature DCs are specialized for naive T-cell activation and are important for cellular immune response.[21] Cytokines such as IL-10 and IL-12, produced during DC maturation, determine whether a Th1 or Th2 immune response will be generated. Mature DCs release IL-12, which stimulates a Th1 immune response, but IL-10 blocks DC maturation. We assessed the effects of ZXL1 on production of IL-10 and IL-12 by mouse DCs during *M. tb*/ManLAM stimulation (**Figure 5a**,**b**). When DCs were stimulated by LPS plus iH37Rv/ManLAM, IL-10 production was increased but IL-12 production was decreased, compared with stimulation by LPS alone (**Figure 5a**,**b**). When DCs were stimulated in the presence of ZXL1, IL-10 secretion was decreased by 42–44% and IL-12 production was increased by 82–87%, compared with LPS plus iH37Rv/ManLAM stimulation (**Figure 5a**,**b**). The control aptamer ZXL4, which showed the weakest binding to ManLAM, did not affect the production of IL-10 and IL-12 (**Figure 5a**,**b**). Moreover, in LPS-stimulated human DC groups, ZXL1 decreased IL-10 production by 31–36% and increased IL-12 production by 52–91% (**Supplementary Figure S4a,b**). ZXL1 blocked the suppression of DCs caused by ManLAM, and it enhanced MHC-II expression, reduced IL-10 production, and increased IL-12 production in DCs. Therefore, we proposed that binding of ZXL1 to ManLAM might facilitate DC maturation, antigen presentation, and T-cell activation (**Figures 4** and **5a**,**b**).

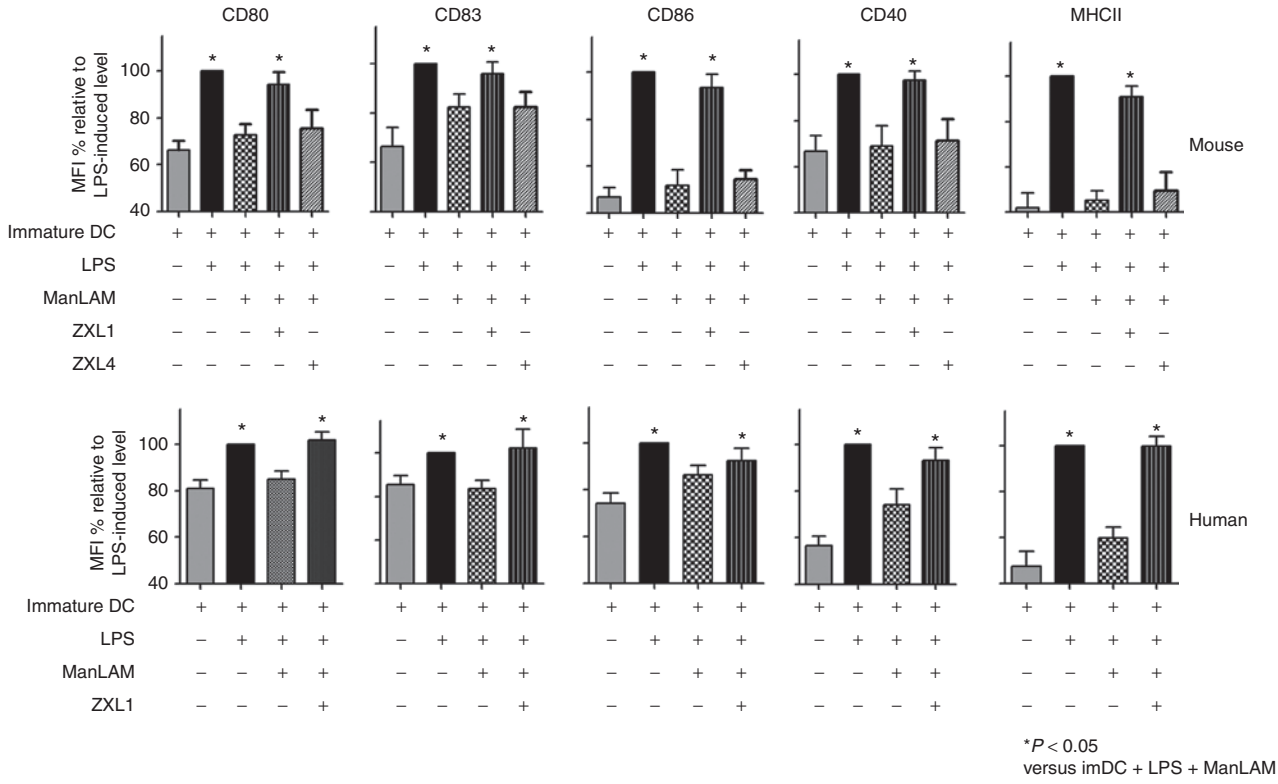

Figure 4 ZXL1 enhanced the maturation of mouse and human dendritic cells (DCs). Immature DCs were stimulated with LPS (1 μg/ml) plus *Mycobacterium tuberculosis* (*M. tb*) H37Rv (1×10^7 colony forming units (CFUs) per 10^6 DCs)/mannose-capped lipoarabinomannan (ManLAM) (10 μg/ml) in the presence or absence of aptamer ZXL1 (5 μmol/l) for 24 hours. The expression of CD80, CD83, CD86, CD40, and major histocompatibility complex II (MHC-II) on DCs was determined by flow cytometry. Mean fluorescence intensities were normalized to the values obtained for stimulation with LPS alone and were expressed as percentages. *$P < 0.05$ versus immature DC + LPS + ManLAM. All data are shown as the means ± SEMs ($n = 3$).

© The American Society of Gene & Cell Therapy

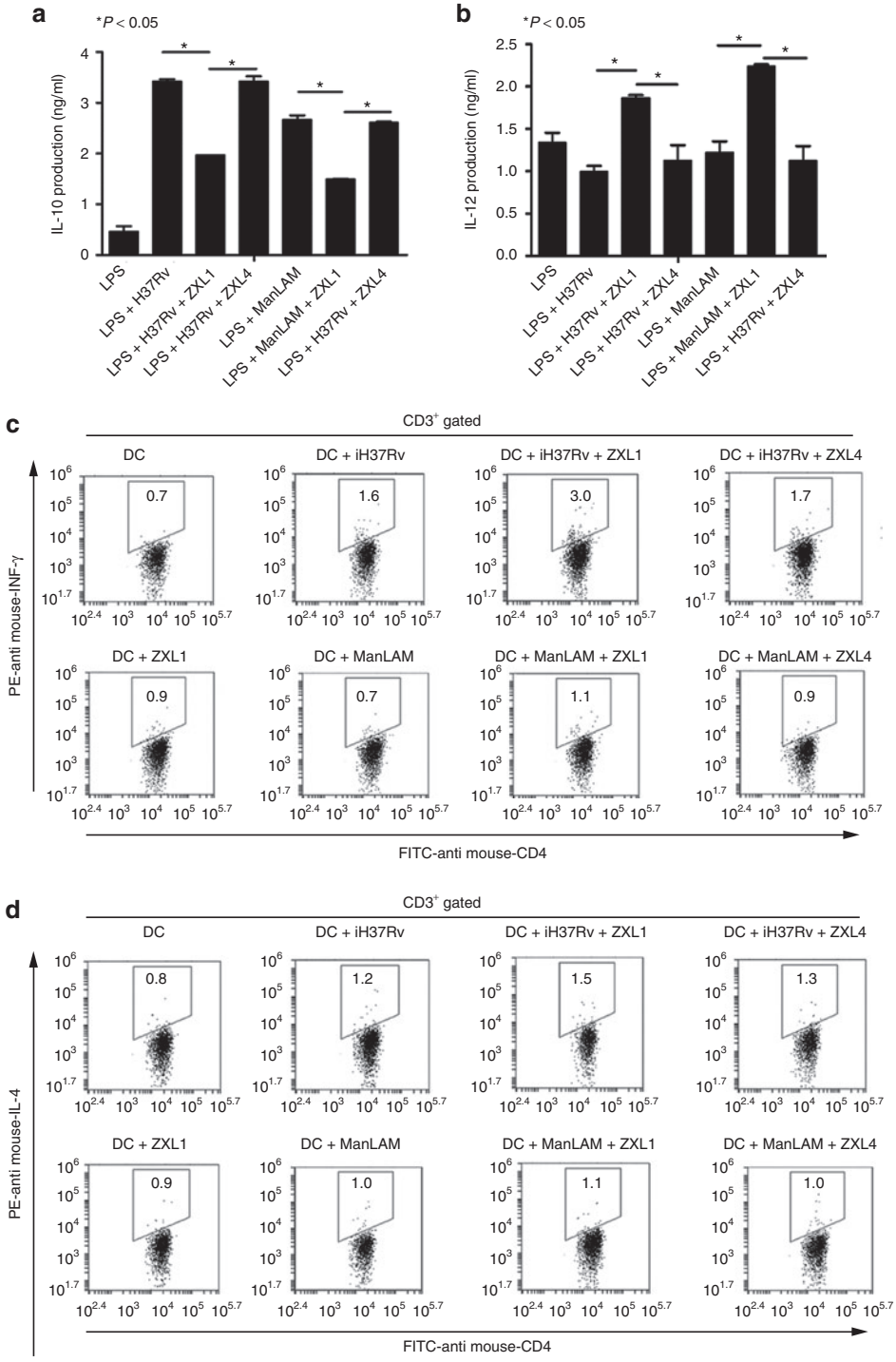

Figure 5 ZXL1 enhanced antigen presentation by dendritic cells (DCs). (**a**,**b**) Immature mouse DCs (2×10^6 cells/ml) were cultured for 24 hours with LPS (1 μg/ml) or LPS plus iH37Rv (1×10^6 colony forming units (CFUs)/ml)/mannose-capped lipoarabinomannan (ManLAM) (10 μg/ml) in the presence or absence of ZXL1 (5 μmol/l). Supernatants were collected and analyzed for interleukin (IL)-10 and IL-12 production by enzyme-linked immunosorbent assay. (**a**) IL-10 secretion by *Mycobacterium tuberculosis* (*M. tb*) H37Rv/ManLAM-stimulated DCs. *$P < 0.05$ versus LPS+iH37Rv/ManLAM or LPS+iH37Rv/ManLAM+ZXL4. All data are shown as the means ± SEMs ($n = 3$). (**b**) IL-12 secretion by *M. tb* H37Rv/ManLAM-stimulated DCs. *$P < 0.05$ versus LPS+iH37Rv/ManLAM or LPS+iH37Rv/ManLAM+ZXL4. All data are shown as the means ± SEMs ($n = 3$). (**c**,**d**) Naive $CD4^+$ T cells were purified from mouse splenocytes using antibody-coupled microbeads and a MACS separator. ZXL1-treated-*M. tb* H37Rv/ManLAM-pulsed DCs (0.5×10^6) were cocultured with 1×10^6 naive $CD4^+$ T cells for 5 days. IFN-γ and IL-4 production by $CD4^+$ T cells was determined by flow cytometry. (**c**) IFN-γ production by $CD4^+$ T cells stimulated by DCs pulsed with ZXL1-treated-iH37Rv/ManLAM. (**d**) IL-4 production by $CD4^+$ T cells stimulated by the DCs pulsed with ZXL1-treated-iH37Rv/ManLAM. IFN, interferon; PE, R-phycoerythrin.

© The American Society of Gene & Cell Therapy

We then assessed the effects of ZXL1 on naive CD4$^+$ T-cell cytokine production, which was induced by antigen-presenting *M. tb*/ManLAM-specific DCs. IH37Rv/ManLAM was loaded onto the DCs in the presence of ZXL1, and stimulated DCs were cocultured with naive CD4$^+$ T cells. The resultant IFN-γ and IL-4 production by CD4$^+$ T cells was determined by FCM. As expected, IFN-γ, a Th1-type cytokine, was increased by the DCs pulsed with ZXL1-treated-iH37Rv/ManLAM compared with the action by iH37Rv/ManLAM-pulsed DCs (**Figure 5c**). However, a Th2-type cytokine, IL-4, was minutely increased by the DCs pulsed with ZXL1-treated-iH37Rv, and IL-4 production by ZXL1-treated ManLAM group was similar to that produced by the ManLAM-only group (**Figure 5d**). Cytokine production by the control CD4$^+$ T cells was almost unchanged in the immature DC or ZXL1-treated immature DC groups (**Figure 5c**,**d**). Cytokine production in the ZXL4-treated-iH37Rv/ManLAM group was slightly increased, probably due to the effects of nonspecific ssDNA (**Figure 5c**,**d**). These data indicated that binding of ZXL1 to ManLAM upregulated DC presentation of iH37Rv antigens for Th1 naive CD4$^+$ T-cell activation, perhaps facilitating cellular immunity against *M. tb.*

ZXL1 prevented *M. tb* H37Rv infection in mice

To evaluate the effects of ZXL1 during *M. tb* infection, BALB/c mice were aerogenically challenged with *M. tb* H37Rv and treated with ZXL1. Streptomycin was used as a positive therapeutic control (**Figure 6a**–**e**). Thirty days after infection, ZXL1 treatment significantly reduced the *M. tb* H37Rv load in mouse lungs and spleens compared with the loads in the phosphate-buffered saline (PBS) and ZXL4 control groups (**Figure 6a**,**b**). Compared with the NK2 aptamer, which was previously reported as a potential anti-*M. tb* treatment,[22] the ZXL1 group had significantly lower *M. tb* H37Rv colony-forming units (CFU) in lungs and spleens (**Figure 6**,**b**; $^*P < 0.05$), which suggested that ZXL1 treatment elicited much better protection against *M. tb* infection. Large numbers of *M. tb* H37Rv were observed in lung and spleen tissues from PBS and ZXL4 control groups, whereas few bacteria were found in the ZXL1 treatment group (**Figures 6c**). Histopathological analysis of alveolar tissue from ZXL1 group showed that the number and size of granulomas were smaller, and it was mostly intact with only mild signs of alveolitis, a small amount of lymphocyte infiltration and granulomatous inflammation, and a few red blood cells present in connective tissue. By contrast, necrotic and proliferative granulomas were observed in PBS and ZXL4 control groups (**Figure 6d**).

Histological examination of splenic tissues demonstrated clearly evident lymphoid white pulp and red pulp in ZXL1-treated mice, whereas the white pulp and red pulp areas in PBS and ZXL4 control groups were completely disorganized, with many basophilic granules and necrotic cellular debris (**Figure 6e**). These data suggested that ZXL1 alleviated the pathology due to and prevented *M. tb* H37Rv infection in mice.

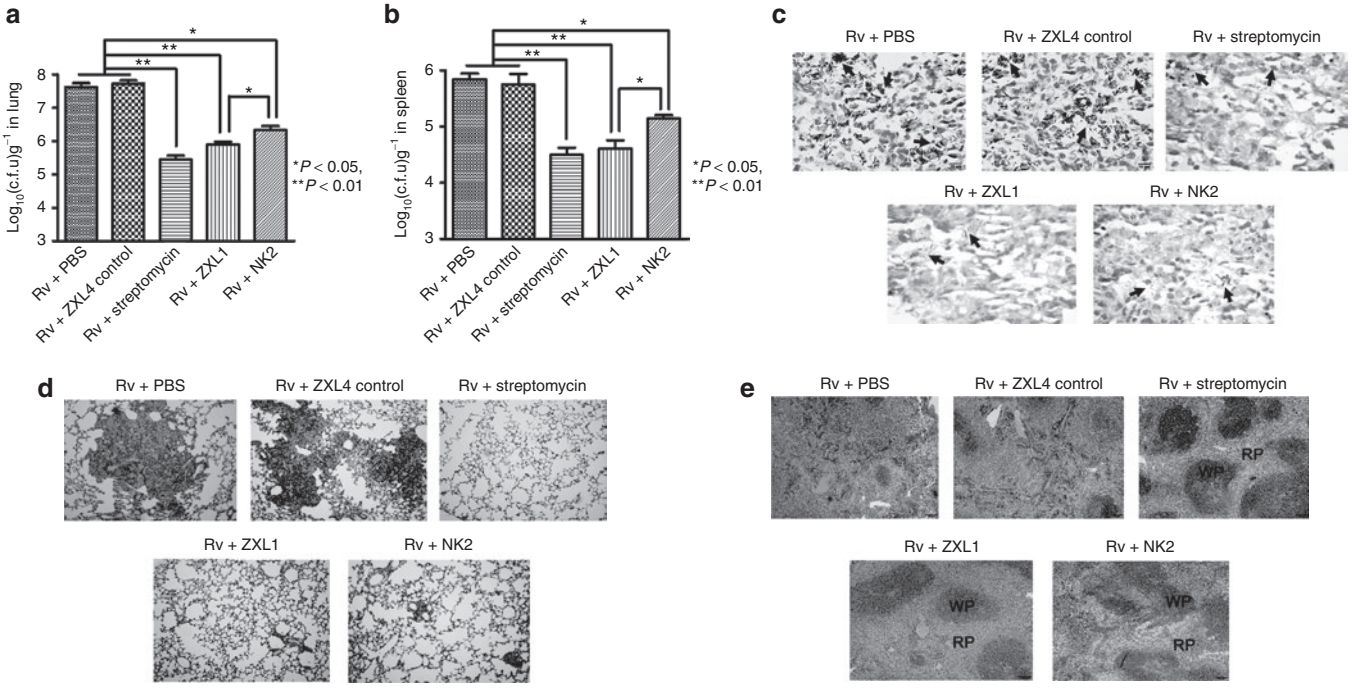

Figure 6 ZXL1 prevented *Mycobacterium tuberculosis* (*M. tb*) H37Rv infection in mice. BALB/c mice were infected with *M. tb* H37Rv by an inhalation exposure system to deposit 100 CFUs of bacteria in the lungs. From day 3, ZXL1/NK2 were administered thrice i.v. into the mice once every 3 days (1 μmol/l × 3 per mouse) ($n = 6$ per group). Control treatments were i.v. injections with ZXL4 thrice (1 μmol/l × 3 per mouse) or i.m. injections streptomycin daily for a week (200 μg × 7 per mouse). (**a**) *M. tb* CFU assay in lung. After 30 days of *M. tb* infection, mice were sacrificed; the numbers of *M. tb* CFUs in lungs were counted. (**b**) *M. tb* CFU assay in spleen. (**c**) Ziehl-Neelsen acid-fast stain analysis. Lung tissue sections were analyzed with Ziehl-Neelsen acid-fast staining. Arrows indicate the positive bacteria (1,000×). (**d**) Histopathology. Lung tissues were stained with hematoxylin and eosin (H&E) and evaluated by light microscopy (100×). (**e**) Histopathology. Spleens were stained with H&E and evaluated by light microscopy (100×). PBS, phosphate-buffered saline.

© The American Society of Gene & Cell Therapy

ZXL1 prevented chronic *M. tb* H37Rv infection in rhesus monkeys

M. tb pathogenesis and the ability of host immunity to challenge infection differ among mice and rhesus monkeys. *M. tb*-infected mice develop granulomatous inflammation in their lungs, but in primates, TB granulomas are well organized and more compact.[23] Anti-TB agents are usually effective against TB in monkeys, as indicated by: (i) prolonged survival or decreased *M. tb* CFUs in lungs, (ii) prevention of increases in erythrocyte sedimentation rates (ESRs) and C-reactive protein (CRP), (iii) weight gain, and (iv) improvement in chest X-ray findings, which closely mimic the symptoms of human TB disease.[24,25] Therefore, we used the rhesus monkey model of TB to assess ZXL1 *in vivo*. A total of seven rhesus monkeys were randomly divided into three groups as follows: two monkeys in the PBS group, two monkeys in the streptomycin group, and three monkeys in the ZXL1 group.

During infection, the concentrations of ESR and CRP were monitored and determined to evaluate the extent of acute inflammation.[24,25] Because a total of seven rhesus monkeys were used in three groups, we did not use statistical analysis to compare data from these three groups. As shown in **Figure 7a**,**b**, in the PBS group, *M. tb* infection remarkably increased ESR and CRP concentrations, whereas there were almost no changes of ESR and CRP concentrations in the ZXL1 treatment group. These data implied that ZXL1 treatment prevented acute inflammation during *M. tb* infection. Body weight loss was observed in the PBS group, but ZXL1 treatment reduced weight loss (**Figure 7c**). The number of *M. tb* H37Rv CFUs in rhesus monkey lungs was determined at 16 weeks postinfection (**Figure 7d**). Both ZXL1 and streptomycin treatments reduced the *M. tb* infection in lungs compared with the PBS treatment.

To evaluate effects of ZXL1 on pulmonary TB, chest radiographic examinations were performed before and after infection (**Figure 7e** and **Supplementary Table S3**). Two out of three monkeys contained pathological nodules in the right lung before ZXL1 treatment, but these nodules were absorbed at week 16 after ZXL1 treatment. Active pulmonary TB developed in the third monkey treated with ZXL1 (**Figure 7e** and **Supplementary Table S3**). Both PBS-treated monkeys showed active pulmonary TB, with lung parenchymal abnormalities including nodule(s), consolidation, and cavities (**Figure 7e** and **Supplementary Table S3**). One of the two streptomycin-treated monkeys showed active pulmonary TB at week 16, but the other showed atypical pulmonary lesions (**Figure 7e** and **Supplementary Table S3**).

Hematoxylin-and-eosin staining revealed that the pulmonary inflammation in the PBS group was granulomatous, with epithelioid macrophages, Langhans giant cells, lymphocytes, and a characteristic caseous, necrosis center (**Figure 7f**). Chronic lung inflammation and interstitial pneumonia were found, but no granulomas were observed in the ZXL1 and streptomycin

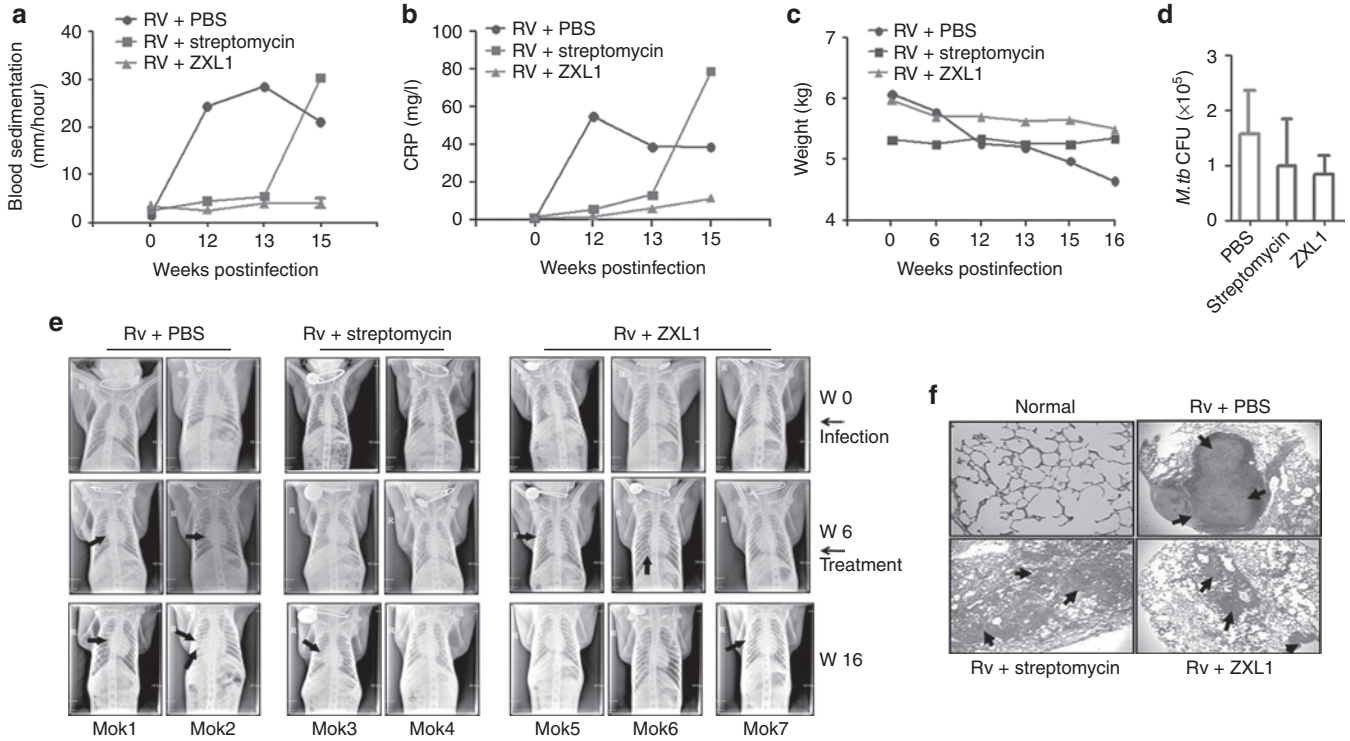

Figure 7 ZXL1 prevented *Mycobacterium tuberculosis* (*M. tb*) H37Rv infection in rhesus monkeys. A total of seven rhesus monkeys were intratracheally infected with 100 colony-forming units (CFUs) of *M. tb* H37Rv at week 0. At week 6, infected monkeys were randomly divided into three groups as follows: two monkeys in the phosphate-buffered saline (PBS) group, two monkeys in the streptomycin group, and three monkeys in the ZXL1 group. For the ZXL1 group, monkeys were i.v. injected with ZXL1 (20 µmol/l or 100 µl/kg per monkey) three times per week for 4 weeks. For the streptomycin group, monkeys were i.m. injected with streptomycin (20 mg/kg per day) for 30 days. (**a**) Blood sedimentation determination. (**b**) C-reactive protein (CRP) determination. (**c**) Body weights of infected monkeys. (**d**) *M. tb* CFU assay. (**e**) Chest X-ray detection. The arrows indicate the pulmonary lesions. (**f**) Histopathology. Lung tissue sections were stained with hematoxylin and eosin and evaluated by light microscopy (100×). PBS, phosphate-buffered saline.

© The American Society of Gene & Cell Therapy

treatment groups (**Figure 7f**). These data indicated that ZXL1 treatment hindered infection in rhesus monkeys.

DISCUSSION

Recently, ssDNA aptamers against MPT64 and CFP-10-ESAT-6 were also reported for TB diagnostic research purposes.[26,27] We are the first to use aptamers as therapeutic agents against virulent *M. tb*.[22] We previously used whole-bacterium SELEX to generate a therapeutic aptamer, NK2, against virulent *M. tb*.[22] The ZXL1 aptamer that was identified in this study has several advantages relative to the NK2 aptamer, although they have similar binding affinities to H37Rv strain. First advantage, the target molecule ManLAM of ZXL1 aptamer is clear; however, the molecule on the surface of *M. tb* H37Rv bacteria that is targeted by the NK2 aptamer remains elusive. Second, we have compared these two aptamers in an *in vivo* study, and we found that ZXL1 was more effective than NK2. Our results confirmed that the ZXL1 mouse group had significantly lower *M. tb* H37Rv CFUs in lung and spleen compared with the NK2 group (**Figure 6a**,**b**), which suggested that ZXL1 was more effective as a therapeutic agent against virulent *M. tb* H37Rv than NK2 (**Figure 6a**–**e**).

Importantly, ZXL1 did not bind to BCG, which had a ManLAM component on its surface, indicating that ZXL1 specifically targeted the ManLAM from *M. tb* H37Rv (**Figures 2b**,**c**). There is some variation in acyl forms and phosphates of ManLAM from *M. tb* H37Rv and BCG.[28] ZXL1 might specifically bind to unique acyl forms and phosphate structures on ManLAM of *M. tb* H37Rv.

The ManLAM-binding residues present on MR and DC-SIGN have not yet been identified. Few studies about the interaction between ManLAM and DC MR have been reported. ManLAM has its hydrophilic domain defined as a rigid, linear, and, in some cases, large structure with multiple branches.[29] Therefore, it is possible that the hydrophilic fragments from MR/DC-SIGN might interact with the hydrophilic domain of ManLAM. We chose the highly hydrophilic amino acid fragments MRp2 (CRD4 domain), human/mouse MRp1 (Cys-MR domain), and DC-SIGN p1/2 from CRDs of DC-SIGN as competitors in ELONA, and our data suggested that human MRp1 and MRp2 interacted with ManLAM (**Figure 3a**,**b**). The ZXL1-binding site may be in the ManLAM domain, which is recognized by CRD4 of MR.

However, we have not examined whether other domains of MR and DC-SIGN might be involved in disruption of binding of ZXL1 to ManLAM. In our future studies, we will use the full-length MR and DC-SIGN proteins—as well as various amino acid fragments of MR and DC-SIGN—as competitors to demonstrate the details of ZXL1-mediated interference with ManLAM-MR/DC-SIGN interaction. Because the aptamer ZXL1 specifically

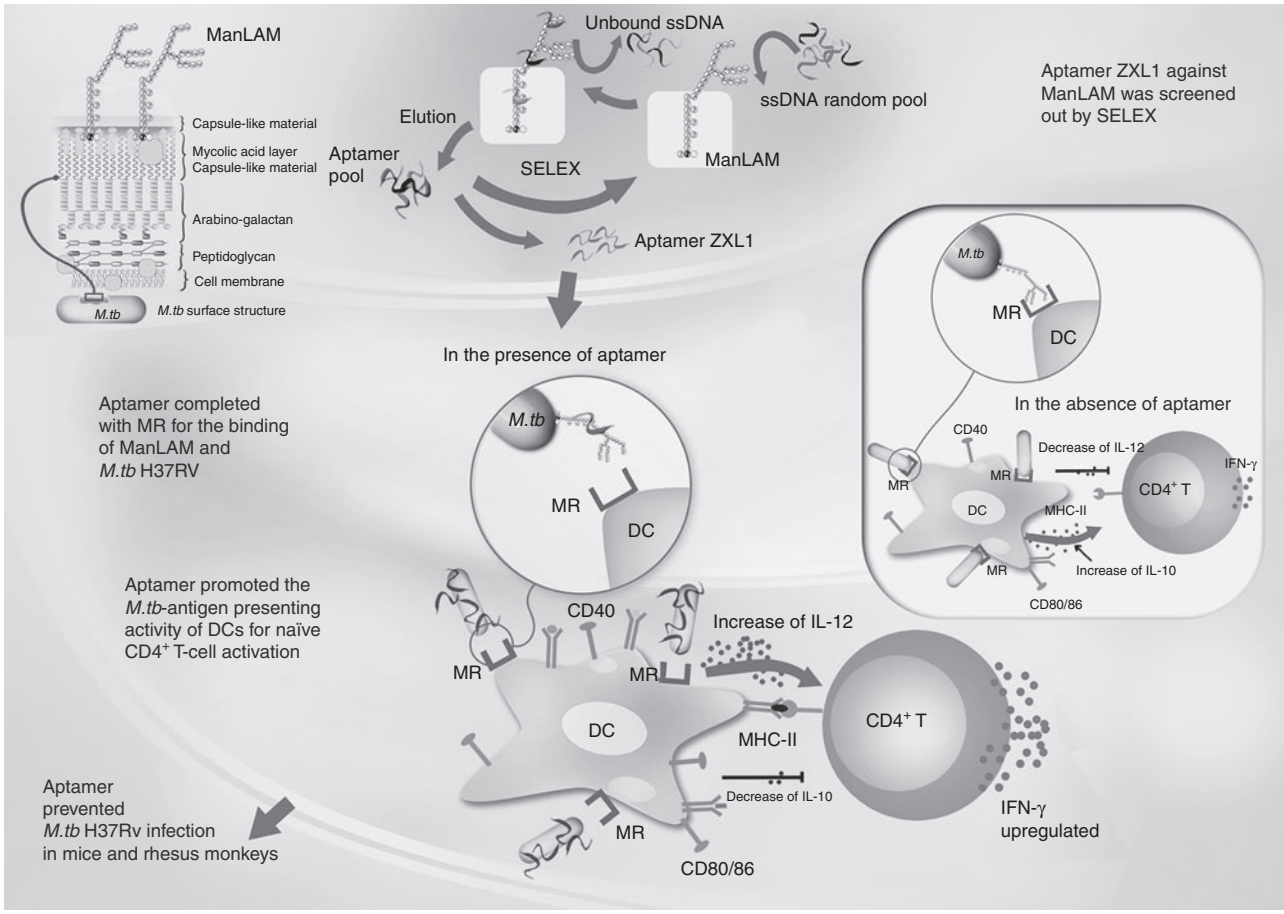

Figure 8 Putative model of aptamer ZXL1-mediated blocking of H37Rv mannose-capped lipoarabinomannan (ManLAM)-induced immunosuppression. DC, dendritic cell; IFN, interferon; IL, interleukin; MHC, major histocompatibility complex; MR, mannose receptor; *M. tb*, *Mycobacterium tuberculosis*; SELEX, systematic evolution of ligands by exponential enrichment; ssDNA, single-stranded DNA.

© The American Society of Gene & Cell Therapy

binds to ManLAM, whose potential receptor might be MR, we speculate that the binding affinities of ManLAM/iH37Rv to various receptors on DCs, such as Toll-like receptor 2, CD14, CD1b, scavenger receptor, and complement receptors, might be not as strong as the interaction between ManLAM and MR. The effects of ZXL1 on various receptors could be determined in future studies.

ManLAM binds DC-SIGN and blocks DC maturation and $CD4^+$ T-cell activation.[5,6,8] Here, our results suggested that ManLAM bound to MRp2 and blocked DC maturation. Aptamer ZXL1 against ManLAM promoted DC maturation by blocking ManLAM-mediated immunosuppression of DCs. Our results showed that ZXL1 treatment promoted the expression of MHC-II and costimulatory molecules (CD40, CD80, CD83, and CD86) on DCs, decreased IL-10 production, and increased IL-12 production (**Figures 4** and **5a**,**b**). More importantly, ZXL1-mediated disruption of MR binding to ManLAM enhanced antigen presentation by DCs and functional naive $CD4^+$ T-cell responses (**Figure 5c**,**d**).

According to our results shown in **Figure 4**, ZXL1 had higher effect in terms of ManLAM-mediated prevention of LPS-induced DC maturation in murine DCs than in human DCs (**Figure 4**). However, we have also observed that ZXL1 competed much better with both mouse- and human-derived MRp2 (**Figure 3a**). Our results shown in **Figure 4**, **3a**, indicate that MRp2 peptide of DCs (common in both human and mouse) might be a more important region involved in the effect of ZXL1 on ManLAM-mediated prevention of LPS-induced DC maturation. Additionally, DC maturation is a complex process and is regulated by different signaling pathways.[30] Murine DCs and human DCs are heterogeneous.[31,32] Therefore, these factors might influence the divergence between human DC maturation and mouse DC maturation.

Despite the high cost of monkey experiments, we used a total of seven monkeys in our study. MHC gene polymorphism possibly led to differences in *M. tb* susceptibility and ZXL1 (or streptomycin) treatment outcomes among monkeys. Although two of the three monkeys recovered from TB after ZXL1 treatment, both the monkeys in the PBS group developed active pulmonary TB. These data suggested that ZXL1 had remarkable anti-TB activity in monkeys.

In this study, the aptamers were dissolved in PBS and were directly administered i.v. into the mice. Whether the modified and formulated aptamers have better effects and are more stable *in vivo* would need to be investigated in future. Our results demonstrated that ZXL1 had almost no toxicological effects on lymphocytes *in vitro* (**Supplementary Figure S5**). There is very limited information on the toxicological properties of aptamers.[13,33] A targeted anti–vascular endothelial growth factor RNA aptamer (Macugen, Pfizer, New York, NY), the first US Food and Drug Administration–approved antiangiogenic agent, underwent a limited toxicological assessment.[34] More assays of toxicological and therapeutic effects of aptamers would be needed in the future study.

The first-line treatment for active TB is a standard 6- to 8-month course of antimicrobial drugs in combination (isoniazid, rifampin, pyrazinamide, ethambutol, and streptomycin).[35,36] Most of these anti-TB drugs target enzymes that inhibit biosynthesis of mycolic acids and fatty acids, obstruct the formation of cell wall, and interfere with DNA-dependent RNA polymerase activity.[35,36] However, there is still increasing prevalence of multidrug-resistant TB in the world today. ZXL1 directly targets ManLAM—a major lipoglycan in the cell wall of *M. tb*—and interferes with the recognition of ManLAM by host DC MR, resulting in prevention of ManLAM-induced immunosuppression and augmentation of *M. tb*-antigen presentation for naive $CD4^+$ T-cell activation (**Figure 8**). The antimycobacterial mechanism of aptamer ZXL1 is different from those of well-known antimicrobial drugs, which usually target bacterial enzymes and easily cause drug-resistant *M. tb* strains. We expect that ZXL1 can be used as a new anti-TB drug candidate without cross-resistance with known antimycobacterial agents.

MATERIALS AND METHODS

Bacteria and animals. *M. tb* H37Rv (strain American Type Culture Collection (ATCC) 93009) and BCG (strain ATCC 35734) were purchased from the Beijing Biological Product Institute (Beijing, China). *M. tb* H37Rv and BCG were maintained on Lowenstein–Jensen medium and harvested while in the log phase of growth. Bacilli were washed in PBS containing 0.05% Tween-80 and triturated uniformly before use.[37] *M. smegmatis* (strain ATCC 70084), *M. intracellulare* (strain ATCC 13950), *M. avium* (strain ATCC 25291), *P. aeruginosa* (strain ATCC 27853), *S. aureus* (strain ATCC 25923), *E. coli* (strain ATCC 25922), *S. albus* (strain ATCC 20237), *M. luteus* (strain ATCC 10240), and *S. typhimurium* C5[38] were propagated from laboratory stocks (School of Medicine, Wuhan University, Wuhan, China). Female BALB/c mice (5–6 weeks old) and female rhesus monkeys of Chinese origin (3–6 years old, obtained from the Animal Laboratory Center, Wuhan University) were used in *M. tb* challenge experiments. All bacterial cultures and animal tests were carried out in the Animal Biosafety Level 3 Laboratory (ABSL-III) of the Wuhan University School of Medicine. The protocols for bacterial challenge were performed in compliance with all guidelines and were approved by the Institutional Animal Care and Use Committee of Wuhan University.

ManLAM preparation. ManLAM was extracted and purified from delipidated cells as previously described.[15] Purified ManLAM fractions were analyzed by sodium dodecyl sulfate–polyacrylamide gel electrophoresis, silver staining, and western blotting. Biotin-labeled ConA (Sigma, St Louis, MO), which specifically binds mannose, was used to probe the western blots, which were subsequently incubated with horseradish peroxidase–conjugated streptavidin. The color was developed with nitroblue tetrazolium and bromochloroindolyl phosphate.

Aptamer screening. The aptamers were screened using the method described previously.[22] Briefly, the random ssDNA library contained the 88-mer oligonucleotides with the following sequence: 5′-GCGGAATTCTAATACG ACTCACTATAGGGAACAGTCCGAGCC-N30-GGGTCAATGCGTCATA-3′, where the central N30 represented random oligonucleotides based on equal incorporation of A, G, C, and T at each position. At the beginning of *in vitro* selection, 0.04 mg/ml of ManLAM was coated on a 96-well plate and incubated at 37 °C for 2 hours. The well was then washed five times and subsequently blocked with 200 µl of salmon sperm DNA (100 µg/ml) at 37 °C for 1 hour. SsDNAs were mixed with yeast transfer RNA (5 µmol/l) and incubated at 37 °C for 30 minutes. After washing, 50 µl of double-distilled H_2O was added and heated at 99 °C for 10 minutes. The supernatant was used as the template for asymmetric polymerase chain reaction amplification, and then the ssDNA products were used in the next round of selection. We applied the counterselection step by the use of an empty well, followed by the selection of ManLAM from the 3rd to the 10th cycle.

Aptamer cloning, sequencing, and structure analysis. SsDNAs from the 12th round of selection were amplified by polymerase chain reaction to obtain double-stranded DNAs. Double-stranded DNAs were digested with

© The American Society of Gene & Cell Therapy

*Bam*HI and *Eco*RI and subcloned into a pUC19 vector, which was used to transform *E. coli* DH5α bacteria. Selected clones were sequenced. Multiple sequence alignments and secondary analyses were conducted with the DNAMAN software (version 3.2; Lynnon Biosoft, Pointe-Claire, Quebec, Canada). The identified aptamers were named ZXL1–14.

Enzyme-linked oligonucleotide assay. SsDNA aptamers were amplified with a biotin-labeled primer to generate biotin-labeled ssDNA aptamers. Ninety-six-well enzyme-linked immunosorbent assay plates were coated with ManLAM or heat-inactivated *M. tb* H37Rv (iH37Rv, at 65 °C for 30 minutes) and incubated overnight at 4 °C. After blocking with 200 µl salmon sperm DNA (100 µg/ml) at 37 °C for 1 hour, biotin-labeled ssDNA aptamers were added and incubated at 37 °C for 2 hours. Horseradish peroxidase–conjugated streptavidin (1:1,000) was added and incubated for 30 minutes at 37 °C. After adding substrate and stop buffer, absorbance was determined at 450 nm by a microplate reader. In the background control, the ManLAM (or iH37Rv) was coated on the wells, but none of the ssDNA aptamers were added. For each sample, the optical density at 450 nm (OD_{450}) of background control was subtracted from the OD_{450} value of the experimental sample. Washes were performed to remove unbound aptamers in ELONA.

To evaluate specificity of binding of ZXL1, 1×10^5 CFUs of the bacteria were coated onto wells, and 2 µmol/l of biotin-labeled aptamer ZXL1 was added to each well. GraphPad Prism (GraphPad Software) was used to perform nonlinear curve-fitting analysis for K_d and K_i calculation.

Hydrophilic amino acid fragment MRp2 (CRD4 domain), human/mouse MRp1 (Cys-MR domain), and DC-SIGN p1/2 from CRDs of DC-SIGN were analyzed using the DNAMAN software.

Confocal microscopy. To observe the binding between ZXL1 and *M. tb*, iH37Rv/BCG were coated onto slides at 37 °C for 30 minutes. After washing with PBS, samples were incubated with FAM-labeled ZXL1 (5 µmol/l) at 37 °C for 2 hours. After extensive washing with PBS, samples were observed using confocal microscopy.

Flow cytometry. To assess the binding specificity of ZXL1, 1×10^7 CFUs of *M. tb* H37Rv, BCG, and *M. smegmatis* were fixed with 70% ethanol for 10 minutes. Fixed bacteria were incubated with FAM-labeled ZXL1 (5 µmol/l) at 37 °C for 1 hour.

To evaluate the role of ZXL1 on *M. tb* H37Rv/ManLAM-stimulated DCs, mouse bone marrow–derived DCs and human peripheral blood mononuclear cell–derived DCs (isolated from healthy donors) were prepared.[39,40] Bone marrow cells of mouse were isolated from BALB/c mice by flushing tibias and fibulas. After red blood cell lysis, the cells were plated at a density of 1.5×10^6 cells/ml. The cells were differentiated into bone marrow–derived DCs in complete Roswell Park Memorial Institute (RPMI)-1640 medium containing 10 ng/ml of recombinant murine colony-stimulating factor and 10 ng/ml of recombinant murine interleukin-4 for 6 days. Human peripheral blood mononuclear cells were isolated by Ficoll density-gradient centrifugation. Peripheral blood mononuclear cell density was adjusted to 5×10^6 cells/ml. The cell suspension was added to a flask and incubated at 37 °C for 2 hours. Suspended cells were removed, and adherent cells were maintained in complete RPMI-1640 medium containing 20 ng/ml of rhGM-CSF and 10 ng/ml of rhIL-4 for 6–8 days. Immature DCs were confirmed by CD11c staining and FCM. Immature DCs were stimulated with LPS (1 µg/ml) plus *M. tb* H37Rv (1×10^7 CFUs per 10^6 DCs)/ManLAM (10 µg/ml) in the presence or absence of aptamer ZXL1 (5 µmol/l) for 24 hours. The expression of CD80, CD83, CD86, CD40, and MHC-II on DCs was determined by FCM. For T-cell activation assays, naive $CD4^+$ T cells were purified from mouse splenocytes using antibody-coupled microbeads and a MACS separator (Miltenyi Biotec, Bergisch Gladbach, Germany). ZXL1-treated-*M. tb* H37Rv/ManLAM-pulsed DCs (0.5×10^6) were washed thrice and then cocultured with 1×10^6 naive $CD4^+$ T cells in 1 ml medium for 5 days.

Cytokine detection. For cytokine detection, immature human DCs (2×10^6 cells/ml) were cultured for 24 hours with LPS (1 µg/ml) or LPS plus iH37Rv (1×10^6/ml)/ManLAM (10 µg/ml) in the presence or absence of ZXL1 (5 µmol/l). Supernatants were collected and stored at −80 °C until analysis. Supernatants were analyzed for IL-10 and IL-12 production by enzyme-linked immunosorbent assay (eBioscience, San Diego, CA).

Effects of aptamer ZXL1 on TB in mice. BALB/c mice (6–8 weeks old) were infected aerogenically with *M.tb* H37Rv by an Aerosol Generation Device (Glas-col, Terre Haute, IN). Frozen stocks of *M. tb* H37Rv were thawed quickly at 37 °C, centrifuged at 10,000*g* for 10 minutes, and washed two times with PBS containing 0.05% Tween-80. On day 1, mice were infected with *M. tb* H37Rv with the use of an inhalation exposure system to deposit 100 CFUs of bacteria in the lungs. From day 3, ZXL1/NK2 was administered i.v. into the mice three times (injection once every 3 days, 1 µmol/l × 3 per mouse). For aptamer control treatment, mice were injected with ZXL4 three times (injection once every 3 days, 1 µmol/l × 3 per mouse). Streptomycin treatments were i.m. injections with streptomycin (Cat. S9137, Sigma-Aldrich, St Louis, MO) daily for a week (200 µg × 7 per mouse). On day 30, all mice were sacrificed. The lung and spleen samples were homogenized and plated. After 4–6 weeks of culture at 37 °C, the CFUs were counted on a Schuett Colony Quant system (Schuett-Biotec GmbH, Göttingen, Germany). Lung and spleen sections were fixed in 4% paraformaldehyde, and pathological sections were examined with hematoxylin-and-eosin staining. The Ziehl-Neelsen acid-fast stain was used to analyze the bacterial load in lungs.

Effects of ZXL1 on chronic TB in rhesus monkeys. Rhesus monkeys were intratracheally infected with 100 CFUs of *M. tb* H37Rv at week 0. At week 6, infected monkeys were randomly divided into three groups (ZXL1 group, PBS group, and streptomycin group) to receive treatment. For the ZXL1 group, monkeys were i.v. injected with ZXL1 (20 µmol/l or 100 µl/kg per monkey) three times per week for 4 weeks. For the streptomycin group, monkeys were i.m. injected with streptomycin (20 mg/kg per day) for 30 days.

ESR tests were performed with a LENA automated ESR analyzer (CPC Diagnostics, Chennai, India). Blood was collected from the femoral vein. ESR was expressed as the rate of fall in millimeters per hour. CRP from monkey serum was detected with Hitachi 7080 chemistry analyzer (Hitachi, Tokyo, Japan).

Chest radiographs were taken at week 0, week 6, and week 16 with an "Oralix Dental" unit (Philips Medical Systems, London, UK) using cassettes measuring 165 × 215 mm (6·5 × 8·5 inches) fitted with fast screens and medium fast film (Kodak, Hemel Hempstead).

Lungs from rhesus monkeys were sliced and stained with hematoxylin and eosin. Bacterial loads were determined with the Ziehl-Neelsen acid-fast stain.

Statistical analysis. To analyze the maturation markers on DCs, statistical significance was determined with an unpaired, two-tailed Student's *t*-test with Origin software (OriginLab Corporation, Northampton, MA). *P* values less than 0.05 were considered statistically significant. All other data were analyzed with SPSS software (IBM, New York, NY). A Breslow test was used for statistical analysis of survival curves. Differences were considered to be statistically significant for *P* values less than 0.05. Experimental data were analyzed by analysis of variance.

SUPPLEMENTARY MATERIAL

Figure S1. Secondary structure analysis of aptamer ZXL1.

Figure S2. MR/DC-SIGN peptide competitors had no effects on negative control ZXL4.

Figure S3. Carbohydrate competitors had no effects on the aptamer control ZXL4.

Figure S4. ZXL1 decreased IL-10 but enhanced IL-12 secretion by *M. tb* H37Rv/ManLAM-stimulated human DCs.

© The American Society of Gene & Cell Therapy

Figure S5. *In vitro* toxicity analysis of ZXL1.
Table S1. N30 sequences of ZXL1-ZXL14.
Table S2. The peptides used as competitors in competitive ELONA.
Table S3. Chest X-ray assay of *M.tb* H37Rv infected rhesus monkeys at w16.

ACKNOWLEDGMENTS

We thank Wenzhe Ho (Wuhan University Center for Animal Experiment/ABSL-3 Laboratory) for his valuable comments and for reviewing this manuscript. This work was supported by grants from the National Grand Program on Key Infectious Disease (2012ZX10003002-015), National Natural Science Foundation of China (31221061, 31270176 and 31370197), National Outstanding Youth Foundation of China (81025008), the 973 Program of China (2012CB720604), the Program for Changjiang Scholars and Innovative Research Team in University, the Hubei Province's Outstanding Medical Academic Leader Program, the Science and Technology Program of Wuhan (201150530141), the International Science and Technology Cooperation Program of China (2011DFA31030), and Deutsche Forschungsgemeinschaft (Transregio TRR60).
The authors declare that there are patent applications for this work and aptamer sequences.

REFERENCES

1. World Health Organization. (2011). The burden of disease caused by TB Global tuberculosis control 2011. (http://whqlibdoc.who.int/publications/2011/9789241564380_eng.pdf).
2. Svenson, S, Källenius, G, Pawlowski, A and Hamasur, B (2010). Towards new tuberculosis vaccines. *Hum Vaccin* **6**: 309–317.
3. Colijn, C, Cohen, T, Ganesh, A and Murray, M (2011). Spontaneous emergence of multiple drug resistance in tuberculosis before and during therapy. *PLoS ONE* **6**: e18327.
4. Gengenbacher, M and Kaufmann, SH (2012). Mycobacterium tuberculosis: success through dormancy. *FEMS Microbiol Rev* **36**: 514–532.
5. Mortellaro, A, Robinson, L and Ricciardi-Castagnoli, P (2009). Spotlight on Mycobacteria and dendritic cells: will novel targets to fight tuberculosis emerge? *EMBO Mol Med* **1**: 19–29.
6. Fratti, RA, Chua, J, Vergne, I and Deretic, V (2003). Mycobacterium tuberculosis glycosylated phosphatidylinositol causes phagosome maturation arrest. *Proc Natl Acad Sci USA* **100**: 5437–5442.
7. Mahon, RN, Sande, OJ, Rojas, RE, Levine, AD, Harding, CV and Boom, WH (2012). Mycobacterium tuberculosis ManLAM inhibits T-cell-receptor signaling by interference with ZAP-70, Lck and LAT phosphorylation. *Cell Immunol* **275**: 98–105.
8. Geijtenbeek, TB, Van Vliet, SJ, Koppel, EA, Sanchez-Hernandez, M, Vandenbroucke-Grauls, CM, Appelmelk, B *et al.* (2003). Mycobacteria target DC-SIGN to suppress dendritic cell function. *J Exp Med* **197**: 7–17.
9. Ellington, AD and Szostak, JW (1990). *In vitro* selection of RNA molecules that bind specific ligands. *Nature* **346**: 818–822.
10. Tuerk, C and Gold, L (1990). Systematic evolution of ligands by exponential enrichment: RNA ligands to bacteriophage T4 DNA polymerase. *Science* **249**: 505–510.
11. Mayer, G (2009). The chemical biology of aptamers. *Angew Chem Int Ed Engl* **48**: 2672–2689.
12. Wheeler, LA, Trifonova, R, Vrbanac, V, Basar, E, McKernan, S, Xu, Z *et al.* (2011). Inhibition of HIV transmission in human cervicovaginal explants and humanized mice using CD4 aptamer-siRNA chimeras. *J Clin Invest* **121**: 2401–2412.
13. Bouchard, PR, Hutabarat, RM and Thompson, KM (2010). Discovery and development of therapeutic aptamers. *Annu Rev Pharmacol Toxicol* **50**: 237–257.
14. Charlton, J and Smith, D (1999). Estimation of SELEX pool size by measurement of DNA renaturation rates. *RNA* **5**: 1326–1332.
15. Torrelles, JB, Azad, AK and Schlesinger, LS (2006). Fine discrimination in the recognition of individual species of phosphatidyl-myo-inositol mannosides from Mycobacterium tuberculosis by C-type lectin pattern recognition receptors. *J Immunol* **177**: 1805–1816.
16. Leteux, C, Chai, W, Loveless, RW, Yuen, CT, Uhlin-Hansen, L, Combarnous, Y *et al.* (2000). The cysteine-rich domain of the macrophage mannose receptor is a multispecific lectin that recognizes chondroitin sulfates A and B and sulfated oligosaccharides of blood group Lewis(a) and Lewis(x) types in addition to the sulfated N-glycans of lutropin. *J Exp Med* **191**: 1117–1126.
17. Feinberg, H, Mitchell, DA, Drickamer, K and Weis, WI (2001). Structural basis for selective recognition of oligosaccharides by DC-SIGN and DC-SIGNR. *Science* **294**: 2163–2166.
18. Krohn, KA and Link, JM (2003). Interpreting enzyme and receptor kinetics: keeping it simple, but not too simple. *Nucl Med Biol* **30**: 819–826.
19. McGreal, EP, Miller, JL and Gordon, S (2005). Ligand recognition by antigen-presenting cell C-type lectin receptors. *Curr Opin Immunol* **17**: 18–24.
20. Shimizu, K and Fujii, S (2008). An adjuvant role of in situ dendritic cells (DCs) in linking innate and adaptive immunity. *Front Biosci* **13**: 6193–6201.
21. Balkow, S, Heinz, S, Schmidbauer, P, Kolanus, W, Holzmann, B, Grabbe, S *et al.* (2010). LFA-1 activity state on dendritic cells regulates contact duration with T cells and promotes T-cell priming. *Blood* **116**: 1885–1894.
22. Chen, F, Zhou, J, Luo, F, Mohammed, AB and Zhang, XL (2007). Aptamer from whole-bacterium SELEX as new therapeutic reagent against virulent Mycobacterium tuberculosis. *Biochem Biophys Res Commun* **357**: 743–748.
23. Hirayama, Y, Yoshimura, M, Ozeki, Y, Sugawara, I, Udagawa, T, Mizuno, S *et al.* (2009). Mycobacteria exploit host hyaluronan for efficient extracellular replication. *PLoS Pathog* **5**: e1000643.
24. Okada, M, Kita, Y, Nakajima, T, Kanamaru, N, Hashimoto, S, Nagasawa, T *et al.* (2007). Evaluation of a novel vaccine (HVJ-liposome/HSP65 DNA+IL-12 DNA) against tuberculosis using the cynomolgus monkey model of TB. *Vaccine* **25**: 2990–2993.
25. Langermans, JA, Doherty, TM, Vervenne, RA, van der Laan, T, Lyashchenko, K, Greenwald, R *et al.* (2005). Protection of macaques against Mycobacterium tuberculosis infection by a subunit vaccine based on a fusion protein of antigen 85B and ESAT-6. *Vaccine* **23**: 2740–2750.
26. Qin, L, Zheng, R, Ma, Z, Feng, Y, Liu, Z, Yang, H *et al.* (2009). The selection and application of ssDNA aptamers against MPT64 protein in Mycobacterium tuberculosis. *Clin Chem Lab Med* **47**: 405–411.
27. Rotherham, LS, Maserumule, C, Dheda, K, Theron, J and Khati, M (2012). Selection and application of ssDNA aptamers to detect active TB from sputum samples. *PLoS ONE* **7**: e46862.
28. Nigou, J, Gilleron, M and Puzo, G (2003). Lipoarabinomannans: from structure to biosynthesis. *Biochimie* **85**: 153–166.
29. Mishra, AK, Driessen, NN, Appelmelk, BJ and Besra, GS (2011). Lipoarabinomannan and related glycoconjugates: structure, biogenesis and role in Mycobacterium tuberculosis physiology and host-pathogen interaction. *FEMS Microbiol Rev* **35**: 1126–1157.
30. Rescigno, M, Martino, M, Sutherland, CL, Gold, MR and Ricciardi-Castagnoli, P (1998). Dendritic cell survival and maturation are regulated by different signaling pathways. *J Exp Med* **188**: 2175–2180.
31. Banchereau, J and Steinman, RM (1998). Dendritic cells and the control of immunity. *Nature* **392**: 245–252.
32. Shortman, K and Liu, YJ (2002). Mouse and human dendritic cell subtypes. *Nat Rev Immunol* **2**: 151–161.
33. Keefe, AD, Pai, S and Ellington, A (2010). Aptamers as therapeutics. *Nat Rev Drug Discov* **9**: 537–550.
34. US Food and Drug Administration. (2004). Macugen, Pegaptanib Sodium. FDA Pharmacology Review. (http://www.accessdata.fda.gov/drugsatfda_docs/nda/2004/21-756_Macugen_pharmr.pdf)
35. World Health Organization. (2006). Treatment of tuberculosis: guidelines for national programmes, 4th edition (WHO/HTM/TB/2009.420).
36. Jiang, T, Zhan, Y, Sun, M, Liu, S, Zang, S, Ma, Y *et al.* (2011). The novel responses of ethambutol against Mycobacterium smegmatis mc²155 Revealed by proteomics analysis. *Curr Microbiol* **62**: 341–345.
37. Ma, Y, Chen, HD, Wang, Y, Wang, Q, Li, Y, Zhao, Y *et al.* (2011). Interleukin 24 as a novel potential cytokine immunotherapy for the treatment of Mycobacterium tuberculosis infection. *Microbes Infect* **13**: 1099–1110.
38. Ma, Y, Chen, H, Wang, Q, Luo, F, Yan, J and Zhang, XL (2009). IL-24 protects against Salmonella typhimurium infection by stimulating early neutrophil Th1 cytokine production, which in turn activates CD8+ T cells. *Eur J Immunol* **39**: 3357–3368.
39. Singer, K, Morris, DL, Oatmen, KE, Wang, T, DelProposto, J, Mergian, T *et al.* (2013). Neuropeptide Y is produced by adipose tissue macrophages and regulates obesity-induced inflammation. *PLoS ONE* **8**: e57929.
40. Li, DY, Gu, C, Min, J, Chu, ZH and Ou, QJ (2012). Maturation induction of human peripheral blood mononuclear cell-derived dendritic cells. *Exp Ther Med* **4**: 131–134.